Fluctuating interface in a dilute sedimenting suspension

Evgeny S. Asmolov*
Central Aero-Hydrodynamic Institute, Zhukovsky, Moscow region, 140180, Russia
(Received 7 February 2007; revised manuscript received 24 April 2007; published 18 July 2007)

The evolution of large-scale fluctuations in a monodisperse dilute suspension sedimenting in a wall-bounded container is considered on the basis of a continuum model. The case when the velocity fluctuations are comparable with the Stokes settling velocity is studied. Small deformations of the sedimentation front is replaced by a flat interface with a surface force distribution. The front holds position ensuring the vertical fluid velocity across the front to be small. So it acts approximately as a no-slip wall. The mechanisms of the fluctuation decay are the convection of large-scale concentration disturbances and the sedimentation-front deformations.

DOI: 10.1103/PhysRevE.76.016309 PACS number(s): 47.55.P−, 82.70.Kj, 47.11.Kb

I. INTRODUCTION

Hydrodynamic interactions cause velocities of particles sedimenting in a fluid under gravity to fluctuate about the mean. Fluctuations in a dilute suspension with random particle locations were shown [1,2] to grow linearly with a container size L'. The disturbance field induced by a particle in the low-Reynolds-number limit decays at large distances such as r^{-1}. A slow decay of interparticle interactions is a cause of a fluctuation divergence for an infinite system.

In the experiments [3,4], the velocity fluctuations may either converge to finite values as the container sizes increase or decay over the entire time of the experiments [5]. Large-scale vortex structures were observed in many experimental works [4–9]. The effect is due to the hydrodynamic interactions of many particles. The vortex length scale is comparable with the container width initially and then decreases to several tens of interparticle distance [7].

Koch and Shaqfeh [10] suggested that the long-range hydrodynamic interactions are screened because of a nonrandom suspension microstructure. Interactions between three spheres could create a particle deficit near a test sphere. A short-range pair distribution function increases compared to a random distribution for particles with their relative position perpendicular to gravity. The numerical simulations [11] of a homogeneous suspension found no evidence of the proposed long-range microstructure. The short-range distribution was validated using NMR scattering experimental technique [12]. The pair distribution function followed from the measurements is attractive on a range of about one particle diameter.

Different numerical approaches, Stokesian dynamics [13], lattice-Boltzmann model [11,14,15], and point particles [9,16–18] were applied to simulate the particle motion. The simulations of a homogeneous suspension in a cell with periodic boundary conditions in all three directions [11,13] showed the fluctuation divergence in accordance with the theoretical predictions [1,2]. Particle concentration in this case is uniform during sedimentation [10]. However, the concentration must be inhomogeneous in the vertical direction. The inhomogeneity arises because of particle deposition on a bottom wall of a container and a translating interface between suspension and clean fluid, or a sedimentation front. It received much attention recently [9,14–20]. Luke [19] studied the evolution of small density disturbances in a cell with particle density stably stratified in the vertical direction. Based on a continuum model for a particulate phase, he obtained a finite variance in the fluid velocity at $t>0$.

The vertical stratification of the particle concentration near the front is due to three major factors, namely, self-sharpening, the polydispersity of the particle size, and velocity fluctuations. The first effect originates from the dependence of the hindered settling velocity on the volume fraction [21]. In a dilute monosized suspension, the self-sharpening and polydispersity is negligible, and the fluctuations only can result in the front broadening. A significant spreading of the front was obtained by the point-particle simulations [9,16,17] which set impenetrable barriers for particle motion on the bottom wall using the method of images. Other simulations [18] obtained no front broadening. In the experiments [9], the front width grew linearly with time, and the broadening was explained by the polydispersity. The diffusive spreading of the sedimentation front was proposed [16,17] as a mechanism for the fluctuation decay. The hydrodynamic interactions are screened when the stratification exceeds the critical value.

Another mechanism for the fluctuation decay is the convection of large-scale density disturbances [2,9,14,15,18,20]. Lattice-Boltzmann simulations [14,15] found that the top and bottom rigid walls cause the velocity fluctuations to damp. Following an earlier suggestion by Hinch [2] it was concluded that the bottom wall and the interface act as sinks of fluctuation energy. Large-scale concentration fluctuations with wavelengths compared to the container width were found [9] to decay with time faster, and this results in the decay of the velocity fluctuations. The calculations of the Fourier transforms of the pair distribution function (structure factor) [15] and the concentration disturbances [18] showed that fluctuations with smallest horizontal wave vectors are suppressed most significantly. This is equivalent to a long-range deficit in the pair distribution function but characterizes the macroscopic convective rearrangements of large particle clusters rather than the suspension microstructure.

*Also at Institute of Mechanics, Lomonosov Moscow State University, Moscow, Russia. Electronic address: aes@an.aerocentr.msk.su

The simulation methods are computationally demanding, so that the maximum particle number N is usually less than 10^4–10^5. The continuum model of the sedimentation appears suitable for large containers since the calculation procedure does not depend on N, so there are no restrictions on the particle number. It implies that the distribution of discrete particles is smoothed out. It describes the suspension dynamics at length scales large compared to the interparticle distance. It is assumed that the large scales play a key role in the fluctuation evolution while the suspension microstructure is of less importance.

The continuum approach was applied previously [19,20] for a linear case only when the velocity fluctuations are small compared to the Stokes velocity U_s. It was shown [20] that the convection of particle clusters results in deformations of sedimentation-front shape which attenuate density disturbances near the front. This decay mechanism is significant in wide containers. The objective of the present paper is to develop the approach for the regime when the velocity fluctuations are finite. The model takes into account nonlinear convective effects and avoids problems linked to sharp concentration gradients across the front. The paper is organized as follows. In Sec. II, the perturbation methods are applied to derive the equations governing the particle concentration and position of the sedimentation front in a rectangular cell bounded by two no-slip horizontal walls. The equations are solved in terms of Fourier series. The numerical results are discussed in Sec. III. Finally, the results are summarized in Sec. IV.

II. GOVERNING EQUATIONS

Consider the sedimentation of a homogeneous suspension of identical particles in a rectangular container. The cell is bounded by two rigid horizontal walls and periodic in two horizontal directions. The z axis of the laboratory frame of reference is directed upwards, $\mathbf{e}_z$ is a unit vector along the axis. Particles are distributed randomly over the container at $t=0$. They deposit at $t>0$ on an upper surface of compact sediment. An average particle volume fraction ϕ is small, so that the effects due to fluid exclusion, the thickness of the sediment layer, and the slow rising of the sediment surface with a velocity $O(\phi U_s)$ can be ignored.

The dynamics of the suspension is described in terms of the continuous fields of the number concentration, the fluid, and particle velocities. The fields are averaged over a small volume containing a large number of particles. The microscopic motions of individual particles within the volume due to the hydrodynamic interactions of close particles and Brownian diffusion are neglected. The particle velocity in a dilute suspension is assumed to be the sum of the Stokes velocity and the fluid velocity.

The governing equations are nondimensionalized using the height of the container L', the Stokes velocity U_s, and the value $(L')^{-3}$ in order to scale the space coordinates, the fluid velocity $\mathbf{u}(t,\mathbf{r})$, and the number concentration $n(t,\mathbf{r})$, respectively. It is natural to scale the time by the sedimentation time L'/U_s (it will be shown, however, that there are some shorter time scales for large containers). The continuity equation for the particulate phase is then

$$\frac{\partial n}{\partial t} + \nabla \cdot [n(\mathbf{u} - \mathbf{e}_z)] = 0, \tag{1}$$

$$\mathbf{u} = (u_x, u_y, u_z), \quad \mathbf{r} = (x, y, z),$$

$$n(0,\mathbf{r}) = \begin{cases} n^0(\mathbf{r}), & 0 \leqslant z \leqslant 1, \\ 0, & z < 0, \quad z > 1. \end{cases} \tag{2}$$

The equation is coupled with the dimensionless Stokes equations governing the large-scale fluid flow at small Reynolds numbers:

$$\nabla \cdot \mathbf{u} = 0, \tag{3}$$

$$\nabla p - \Delta \mathbf{u} = -f\mathbf{e}_z, \quad f = 6\pi a n, \tag{4}$$

$$\mathbf{u} = 0 \quad \text{on } z = 0;1. \tag{5}$$

The particle effect on the flow is approximated by the volume forces proportional to the local concentration. Note that the dimensionless particle radius a characterizes not a length scale but the intensity of the volume forces.

The continuity equation (1) involves neither diffusive nor stochastic-noise terms [15,17,22]. The system evolves in a deterministic way for given initial conditions. The stochastic behavior is due to the random initial concentration $n^0(\mathbf{r})$. The density fluctuations induce the fluid velocity fluctuations which grow as λ^2 with a wavelength λ [9,11] [see also Eqs. (21) and (22) below]. So large clusters migrate relative to the average flow and should attenuate much faster. Diffusive transport with a constant diffusion coefficient D gives incorrect reverse dependence on the wavelength, $D\nabla^2 n \sim \lambda^{-2}$.

The continuity equation with the initial condition (2) implies that particles may freely cross the walls. As a result one has $n \neq 0$ as $z<0$, $t>0$. However, a finite concentration below the bottom wall does not influence the flow above the wall because of the no-slip condition. Thus, the bottom wall acts as a particle sink rather than a barrier for particle motion [16,17].

The initial fluctuations of particle concentration are $O(N^{1/2})$, i.e., they are small relative to the average concentration n_0^0. So the initial concentration field can be presented in the form

$$n^0 = n_0^0[1 + \varepsilon \nu^0(\mathbf{r})], \tag{6}$$

$$n_0^0 = N^0/V^0 = 3\phi(4\pi a^3)^{-1}, \quad V^0 = L_x L_y z_f^0,$$

$$\varepsilon = (N^0)^{-1/2} \ll 1, \quad \nu^0 = O(1).$$

Here $N^0 \gg 1$ is the initial particle number in the container, L_x and L_y are the suspension sizes in the horizontal directions. We consider the containers of a square cross section, $L_x = L_y = W$. We study either full, $z_f^0 = 1$, or partially filled containers with an initial height of suspension layer $z_f^0 < 1$. Equation (6) is rewritten in the latter case as

$$n^0 = n_0^0[1 + \varepsilon \nu^0(\mathbf{r})]H(z_f^0 - z).$$

The Heaviside step function H is introduced in order to formally partition the cell into the suspension layer below the

sedimentation front and the clean fluid above the front.

The leading-order initial concentration fields, n_0^0 or $n_0^0 H(z_f^0 - z)$, are homogeneous in the horizontal directions. Such fields do not induce fluid flow, i.e., the solution of the equations governing the fluid motion (3)–(5) is $\mathbf{u}_0^0 = 0$. The particle effect on the fluid is balanced by the pressure $p_0^0 = -6\pi a n_0^0 (z_f^0 - z)$. Small density disturbances inhomogeneous in either horizontal or oblique directions cause the fluid motion. A characteristic velocity can be estimated for thin containers as [2]

$$u^\circ \sim (\phi W/a)^{1/2} \sim N^{1/6}\phi^{1/3}W^{1/6} \quad \text{as } W < 1. \tag{7}$$

The particle number N is assumed to be large enough, so that u° is of the order unity or greater.

As the fluid velocity is expected to remain of the same order during the sedimentation process, the concentration, to the leading order, should be nonuniform in the vertical direction only, $n_0 = n_0(z,t)$. The continuity equation governing the basic-flow concentration follows from Eq. (1):

$$\frac{\partial n_0}{\partial t} - \frac{\partial n_0}{\partial z} = 0.$$

Its solution [20],

$$n_0 = n_0^0 H(z_{f0} - z), \quad z_{f0} = z_f^0 - t, \tag{8}$$

is the constant concentration profile below the sedimentation front. The front travels with the Stokes velocity $-\mathbf{e}_z$.

One can seek a two-term solution of Eq. (1) in the form similar to Eq. (8),

$$n = n_0^0[1 + \varepsilon \nu_1(t,\mathbf{r})]H(z_f - z) \tag{9}$$

$$\equiv n_0^0(1 + \varepsilon\nu_1)H(z_{f0} - z) + n_0^0(1 + \varepsilon\nu_1)[H(z_f - z) - H(z_{f0} - z)]. \tag{10}$$

The expansion takes into account not only the bulk density disturbances but also the variation of the local position $z_f(t,x,y)$ of the sedimentation front. The concentration field with the average front position $z_{f0}(t)$ [the first term in Eq. (10)] involves only the small volume disturbances $\varepsilon n_0^0 \nu_1$. To the leading order, the flow due to this field is zero. The second term corresponds to the layer between the two fronts, z_f and z_{f0} (see Fig. 1), where the concentration $n \approx n_0^0 \operatorname{sgn}(z_f - z_{f0})$ is finite and either positive (a layer of particles) or negative (a layer of pure fluid). As net density disturbances are expected to remain $O(\varepsilon)$ during the sedimentation process, the thickness of the layer must be small,

$$z_f - z_{f0} = \varepsilon\zeta(t,x,y), \quad \zeta = O(1).$$

Otherwise, if $z_f - z_{f0} = O(1)$, the layer is equivalent to $O(1)$ density inhomogeneities, and it would induce very large, of the order $N^{2/3}\phi^{1/3} \gg u^\circ$, velocity disturbances. Extra or deficit particles in the thin layer can be shifted to z_{f0}. This means that the second term in Eq. (10) can be replaced by a surface density distribution,

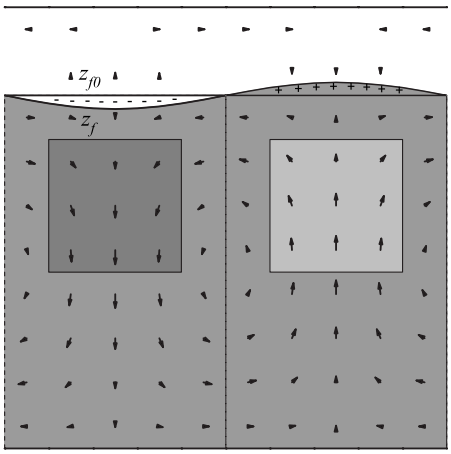

FIG. 1. Sedimentation front above heavy (left square) and light (right square) particle blobs.

$$H(z_f - z) - H(z_{f0} - z) = \varepsilon\zeta\delta(z_{f0} - z) + O(\varepsilon^2),$$

where $\delta = H'$ is the δ function. Then Eq. (9) is rewritten as

$$n = n_0^0[H(z_{f0} - z) + \varepsilon\nu_1 H(z_{f0} - z) + \varepsilon\zeta\delta(z_{f0} - z)] + O(\varepsilon^2). \tag{11}$$

It is uniformly valid for all times provided the front deformations remain small.

The momentum equation (4) with the account of Eq. (11) is rewritten as

$$\nabla p - \Delta\mathbf{u} = -\mathbf{e}_z\gamma[\nu_1 H(z_{f0} - z) + \zeta\delta(z_{f0} - z)],$$

$$\gamma = 6\pi a\sqrt{N^0}/V^0 = O(1). \tag{12}$$

Here the first term in the square brackets is the contribution due to the volume forces. The effect of the thin layer of particles or pure fluid near the interface is equivalent to surface forces (second term) proportional to the layer thickness. The deformations are due to vertical velocity fluctuations. Hence one should also assume that the fluid velocity at the interface is small, $u_{zf} = u_z(t,x,y,z_{f0}) = O(\varepsilon u^\circ)$, to ensure $|z_f - z_{f0}| = O(\varepsilon)$.

Heavy particle blob (left dark square in Fig. 1) induces downward flow in a nearby region. After some time the sedimentation front above such an inhomogeneity will be lower than the basic-flow position z_{f0}, while that for inhomogeneity with reduced concentration (right light square) will be higher. The difference in the weights of the two halves of the container tends to diminish. Thus, the deformation of the front provides the decay mechanism of initial density fluctuations. The deformations cease to grow when the vertical fluid velocity at the interface becomes small. The effects of the volume and surface forces on u_{zf} cancel out.

A. Equations governing disturbances of bulk concentration and front position

Even though the fluctuations of the bulk density and the front position are both small, the convective term $n\mathbf{u}$ in the continuity equation (1) is nonlinear when $u^\circ \sim 1$. The term

describes the convection of large-scale heavy and light clusters, changes in their shapes and magnitudes. The coupling occurs mainly between disturbances with comparable length scales. Large blobs do not transform directly into many small-scale disturbances. Thus, the suspension microstructure and the interactions of close particles are not relevant for large scales.

Substituting the expansion (11) into Eq. (1) and omitting terms $O(\varepsilon^2)$, one has

$$H(z_{f0}-z)\left[\frac{\partial \nu_1}{\partial t}+(\mathbf{u}-\mathbf{e}_z)\cdot\boldsymbol{\nabla}\nu_1\right] + \delta(z_{f0}-z)\left(\frac{\partial \zeta}{\partial t}+u_x\frac{\partial \zeta}{\partial x}+u_y\frac{\partial \zeta}{\partial y}-\varepsilon^{-1}u_z-u_z\nu_1\right) - \delta'(z_{f0}-z)u_z\zeta=0.$$

The last term in the second brackets is out of order compared to $\varepsilon^{-1}u_z$. The last term in the left-hand side can also be neglected as $\partial u_{zf}/\partial z$ is small. Equating separately the first and second terms to zero one obtains the equations governing the disturbances of the bulk concentration,

$$\frac{\partial \nu_1}{\partial t}+(\mathbf{u}-\mathbf{e}_z)\cdot\boldsymbol{\nabla}\nu_1=0, \tag{13}$$

$$\nu_1(0,\mathbf{r})=\nu_1^0=n^0/n_0^0-1,$$

and the disturbances of the front position,

$$\frac{\partial \zeta}{\partial t}+u_{xf}\frac{\partial \zeta}{\partial x}+u_{yf}\frac{\partial \zeta}{\partial y}-u_{zf}\varepsilon^{-1}=0, \tag{14}$$

$$\zeta(0,x,y)=0.$$

The last equation is the Lagrange form of the continuity equation for particles being at the front. It is uniformly valid for short and long times. The velocity at the interface $\mathbf{u}_f$ can be taken at z_{f0}.

The system (3) and (12)–(14) involves four dimensionless groups, namely, γ (or, equivalently, u°) characterizing the magnitude of the fluid velocity, inverse square root of the initial particle number $\varepsilon \ll 1$, and the two geometric parameters, W and z_f^0.

B. Solution in terms of Fourier series

The concentration field of a sedimenting suspension is strongly nonuniform in the vertical direction near the sedimentation front. The difficulties due to Gibbs phenomenon arise when the field is calculated in terms of Fourier series. Nonvertical bulk disturbances and front deformations are small, of order $N^{-1/2}$, relative to the average concentration. However, one should resolve them properly as they only induce the fluid flow. The above decomposition of the bulk and interface motions enables us to avoid the problem.

The solution of the linear (3), (12) and nonlinear (13), (14) equations is constructed in terms of two-dimensional (2D) and 3D Fourier series. The flow is periodic in the two horizontal directions, and all the fields $\mathbf{v}=(\mathbf{u},p,\nu_1,\zeta)$ can be sought for the arbitrary initial distribution ν_1^0 in the form

$$\mathbf{v}=\sum_{k_x,k_y}\mathbf{v}^*\exp[i(k_x x+k_y y)],\quad \mathbf{v}^*(t,z)=(\mathbf{u}^*,p^*,\nu^*,\zeta^*),$$

$$k_l=m_l 2\pi/L_l,\quad m_l=0,\pm1,\pm2,\ldots,\quad l=x,y. \tag{15}$$

The solution for the Fourier coefficients of the velocity field follows to Refs. [18,20]. Substituting expansions (15) into Eqs. (3)–(5) one obtains the system of ordinary differential equations for $\mathbf{v}^*$:

$$i(k_x u_x^*+k_y u_y^*)+\frac{du_z^*}{dz}=0,$$

$$ik_l p^*-\Delta^* u_l^*=0,\quad l=x,y, \tag{16}$$

$$\frac{dp^*}{dz}-\Delta^* u_z^*=-\mathbf{e}_z[f_v^* H(z_{f0}-z)+f_f^*\delta(z_{f0}-z)],$$

$$\mathbf{u}^*=0\quad \text{on } z=0,1,$$

$$\Delta^*=\frac{d^2}{dz^2}-k_\perp^2,\quad k_\perp^2=k_x^2+k_y^2,$$

$$f_v^*=\gamma\nu^*,\quad f_f^*=\gamma\zeta^*.$$

Excluding p^*, u_x^*, and u_y^* one transforms Eqs. (16) into a single equation for the vertical components of the Fourier coefficients:

$$\Delta^{*2}u_z^*=-k_\perp^2[f_v^* H(z_{f0}-z)+f_f^*\delta(z_{f0}-z)], \tag{17}$$

$$u_z^*=\frac{du_z^*}{dz}=0\quad \text{on } z=0;1. \tag{18}$$

The conditions on the sedimentation front are

$$\frac{d^{(i)}u_z^*}{dz^{(i)}}(z_{f0}+0)-\frac{d^{(i)}u_z^*}{dz^{(i)}}(z_{f0}-0)=0,\quad i=0,1,2,$$

$$\frac{d^3u_z^*}{dz^3}(z_{f0}+0)-\frac{d^3u_z^*}{dz^3}(z_{f0}-0)=-k_\perp^2 f_f^*. \tag{19}$$

The jump condition for the third derivative is due to the δ function in the right-hand side of Eq. (17). An arbitrary concentration field can also be expanded in terms of Fourier series in the vertical direction:

$$\nu^*=\sum_{k_z}\tilde{\nu}\exp(ik_z z),$$

$$\nu_1(t,\mathbf{r})=\sum_{\mathbf{k}}\tilde{\nu}\exp(i\mathbf{k}\cdot\mathbf{r}),\quad \mathbf{k}=(k_x,k_y,k_z)=2\pi\mathbf{m}/L_l. \tag{20}$$

Then the solution of the system (16) is

$$\mathbf{u}^* = \begin{cases} \sum_{k_z} \mathbf{b}\tilde{f}_v \exp(ik_z z) + \sum_{j=1}^{4} \mathbf{a}_j^- \varphi_j & \text{as} \quad z \leqslant z_{f0}, \\ \sum_{j=1}^{4} \mathbf{a}_j^+ \varphi_j & \text{as} \quad z > z_{f0}, \end{cases} \tag{21}$$

$$\mathbf{b} = \frac{1}{k^4}(k_x k_z,\ k_y k_z, -k_\perp^2), \quad k^2 = k_x^2 + k_y^2 + k_z^2,$$

$$\mathbf{a}_j^\pm = (a_{jx}^\pm, a_{jy}^\pm, a_{jz}^\pm), \quad a_{3l}^\pm = \frac{ik_l}{k_\perp} a_{3z}^\pm, \quad a_{4l}^\pm = -\frac{ik_l}{k_\perp} a_{4z}^\pm, \quad l = x,y,$$

$$\varphi_{1,2} = \exp(\pm k_\perp z), \quad \varphi_{3,4} = z\exp(\pm k_\perp z). \tag{22}$$

Sixteen unknown constants, $a_{jz}^\pm$, $1 \leqslant j \leqslant 4$, and $a_{jl}^\pm$, $j=1,2$, $l=x,y$ in Eq. (21) are found uniquely in order to satisfy the boundary conditions (18), the no-slip conditions for the horizontal components, and the conditions on the interface (19).

The equation for the 2D Fourier transform of the front position follows from Eq. (14):

$$\frac{\partial \zeta^*}{\partial t} + i \sum_{k_x', k_y'} [\zeta^{*\prime}(k_x' u_{xf}^{*\prime\prime} + k_y' u_{yf}^{*\prime\prime})] - \varepsilon^{-1} u_{zf}^* = 0, \tag{23}$$

where $\zeta'^* = \zeta^*(\mathbf{k}')$, $\mathbf{u}^{*\prime\prime} = \mathbf{u}^*(\mathbf{k}'')$, $\mathbf{k}'' = \mathbf{k} - \mathbf{k}'$.

In order to solve the nonlinear continuity equation (13) in terms of the 3D Fourier series of the concentration $\tilde{\nu}$, one should expand the 2D Fourier transform of the velocity field (21) in terms of 3D Fourier series,

$$\mathbf{u}^* = \sum_{k_z} \tilde{\mathbf{u}} \exp(ik_z z), \tag{24}$$

$$\tilde{\mathbf{u}}(t) = \sum_{k_z'} \left\{ \mathbf{b}' \tilde{f}_v' \int_0^{z_{f0}} \exp[-i(k_z - k_z')z] dz \right\} + \sum_{j=1}^{4} \left[\mathbf{a}_j^- \int_0^{z_{f0}} \varphi_j \exp(-ik_z z) dz + \mathbf{a}_j^+ \int_{z_{f0}}^{1} \varphi_j \exp(-ik_z z) dz \right]. \tag{25}$$

Then the equation governing the 3D Fourier transform of the concentration field can be written as

$$\frac{\partial \tilde{\nu}}{\partial t} - ik_z \tilde{\nu} + i \sum_{\mathbf{k}'} \tilde{\nu}' \mathbf{k}' \cdot \tilde{\mathbf{u}}'' = 0. \tag{26}$$

The sums in Eqs. (23) and (26) correspond to the nonlinear coupling of different modes. Even though the vertical modes with $k_\perp = 0$ do not induce the fluid motion they should be taken into account in the sums.

The systems (23) and (26) with the infinite sums describe exactly the convective motion of the particulate phase provided the effect of finite particle size on the hydrodynamic interactions is neglected. Hence, they are equivalent to the system governing the interactions of point particles. The numerical treatment of the problem requires truncation of the expansions with a number of harmonics great enough to resolve properly the evolution of large-scale fluctuations. The truncated Fourier series result in the smoothing of the concentration and velocity fields. They were applied previously in the point-particle simulations [9,17,18]. It follows from Eqs. (21) and (22) that the velocity Fourier coefficients are proportional to k^{-2}, so a dominant contribution to the velocity fluctuations comes from smaller k. Thus, the coupling between long waves is most important for the velocity fluctuations.

The sums in Eqs. (23), (24), and (26) are truncated at some $m_{\max}$, so that all the modes with $|m_x|$, $|m_y| \leqslant m_{\max}$, $|m_z| \leqslant m_{\max} W^{-1}$ are taken into account. Large $m_{\max}$ makes the sum evaluation computationally expensive. Total number of the modes is $N_m = (2m_{\max}+1)^2(2m_{\max}/W+1) \sim m_{\max}^3$. Each mode may interact with all others, so the number of operations in the convolution sums grows like $N_m^2 \sim m_{\max}^6$. We take $3 \leqslant m_{\max} \leqslant 6$ in the calculations. The point-particle simulations [9], which tried to resolve smaller length scales of the order of the interparticle distance, used $5 \leqslant m_{\max} \leqslant 12$.

The exact velocity field followed from Eq. (21) is smooth on the sedimentation front, unlike the concentration field, and can be approximated well by the truncated 3D Fourier series (24). A relative error is less than 0.04 for the horizontal components in a cubic container and only 0.01 for the vertical one when $m_{\max}=5$.

Fourier coefficients for opposite wave vectors are related by $\tilde{\nu}(\mathbf{k}) = \bar{\tilde{\nu}}(-\mathbf{k})$, $\zeta^*(\mathbf{k}) = \overline{\zeta^*}(-\mathbf{k})$, where the overbar denotes a complex conjugated value. Thus, it is sufficient to solve Eqs. (26) and (23) over a half of Fourier space. The equations are integrated over time using the fourth-order Runge-Kutta routine. The concentration n is evaluated using the inverse Fourier transform (20) and Eq. (9).

An initial inhomogeneous particle concentration in the cell is specified for the random distribution in terms of the concentration Fourier coefficients. The complex values $\tilde{\nu}^0$ are set by the real and imaginary parts distributed normally so that [19]

$$\langle \tilde{\nu}^0 \bar{\tilde{\nu}}^0 \rangle = N^0/(V^0 n_0^0 \varepsilon)^2 = 1, \quad \langle \tilde{\nu}^0 \bar{\tilde{\nu}}^{0\prime} \rangle = 0 \quad \text{as } \mathbf{k} \neq \mathbf{k}'. \tag{27}$$

The ensemble-averaged fluid-velocity fluctuations are evaluated in terms of the 2D Fourier coefficients,

$$\langle u_z^2 \rangle = \frac{1}{L_x L_y} \sum_{k_x, k_y} \langle u_z^* \overline{u_z^*} \rangle, \quad \langle u_\perp^2 \rangle = \frac{1}{L_x L_y} \sum_{k_x, k_y} \langle u_x^* \overline{u_x^*} + u_y^* \overline{u_y^*} \rangle.$$

The fluctuations are calculated over the whole container, not only over a viewing window in the middle part. The relative statistical error of the results averaged over 100 runs is usually less than 0.07.

III. RESULTS

The particle volume content is fixed in the calculations, $\phi = 0.01$, the initial particle number N^0 varies in the range 10^3–10^7. The present theory is applicable when the container is not too tall. The no-slip boundary conditions are satisfied on the horizontal walls only, while for the side walls the

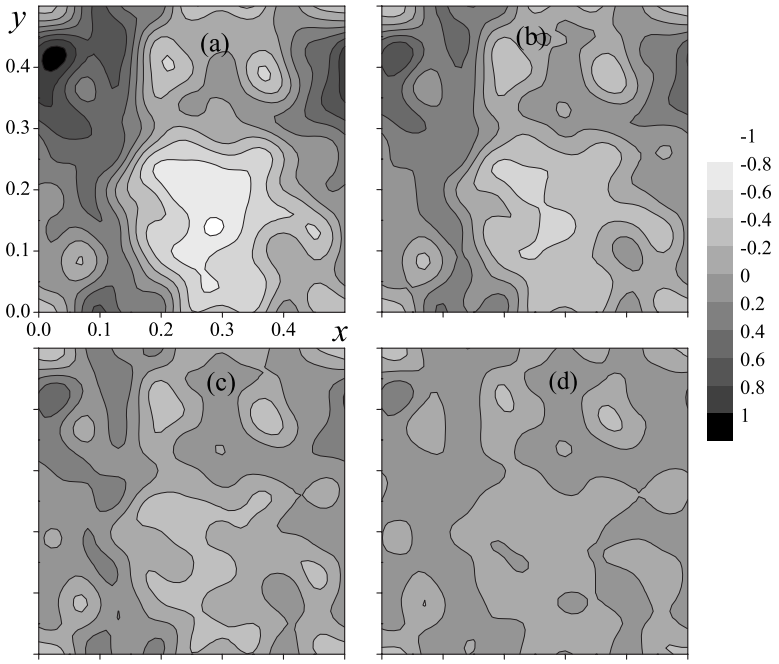

FIG. 2. The vertical fluid velocity across the sedimentation front for the partially filled, $z_f^0=0.8$, container at (a)–(c) $t=0$, 0.005, 0.01, 0.015.

periodic boundary conditions are set. This means that the ensemble-averaged fluctuations $\langle u_z^2\rangle$ and $\langle u_\perp^2\rangle$ do not vary in the horizontal directions. The vertical no-slip walls may play an important role for tall containers [23]. In the experiments [8], parabolic profiles of velocity fluctuations across the cell were observed at small aspect ratios. In the calculations, the container width W varies in the range 1/3–1. Most results are obtained for an elongated container with $N^0=10^5$, $W=0.5$. Then the other dimensionless parameters for the full container are $a=1.81\times10^{-3}$, $u^\circ=1.31$. The maximum number of Fourier modes is usually $m_{\max}=5$, so that the total number of the modes taken into account is $N_m=(2m_{\max}+1)^2(2m_{\max}/W+1)=2541$.

A. Characteristic times

The initial position of the front z_f^0 can be taken arbitrary in the calculations. Characteristic times τ_f it takes for the front to adjust to position ensuring $u_{zf}=O(\varepsilon)$ are different for the full, $z_f^0=1$, and partially filled, $z_f^0<1$, containers.

Simple scaling arguments enable us to estimate the time τ_f^p for the partially filled container. When $z_f^0<1$, the vertical velocity at the interface is finite initially, $u_{zf}\sim u^\circ$. It remains finite during a short time required for the front to translate a distance $O(\varepsilon)$ relative to the basic front position z_{f0}. This time can be estimated as

$$\tau_f^p=\varepsilon/u^\circ=N^{-2/3}\phi^{-1/3}W^{-1/6}\ll 1.$$

For the full container, $z_f^0=1$, the time τ_f^f of the front deformation is greater. The sedimentation front is close to the upper wall at short times. The fluid velocity is small there, $u_z=\partial u_z/\partial z=0$ on $z=1$ because of the no-slip conditions. So the velocity can be estimated near the wall as $u_z\sim u^\circ(1-z)^2/W^2$. The front translates initially with the constant velocity $-\mathbf{e}_z$, and $z_f\simeq 1-t$. Hence, the disturbance velocity at the interface u_{zf} slowly grows with time such as $u^\circ t^2/W^2$. The disturbance of the front position at short times then can be estimated as $\zeta\sim u^\circ t^3/\varepsilon W^2$. It becomes of the order unity at a time

$$\tau_f^f=(\varepsilon W^2/u^\circ)^{1/3}=N^{-2/9}\phi^{-1/9}W^{11/18}.$$

Another time scale is a time τ_c it takes for blobs to translate distances compared to the container height. The convection time is

$$\tau_c=1/u^\circ=N^{-1/6}\phi^{-1/3}W^{-1/6}.$$

The above estimations are rather conventional. However, both times are small compared to the sedimentation time, τ_f, $\tau_c\ll 1$, and $\tau_f<\tau_c$ for large containers as $N\gg 1$. The time step for the numerical integration of Eqs. (26) and (23) is $\Delta t=0.01\tau_f^f$.

For the partially filled container, the characteristic time of the front deformation is very small, $\tau_f^p=2.42\times10^{-3}$, compared to the convection time $\tau_c=0.765$ when $N^0=10^5$, $W=0.5$. The temporal behavior of the vertical fluid velocity across the interface is shown in Fig. 2 for the random concentration field and container with the initial height of the suspension $z_f^0=0.8$. The velocity disturbances are finite initially and decay very fast. So the front does act as the no-slip wall at $t>\tau_f^p$. In the full container with $z_f^0=1$, the time $\tau_f^f=0.0846$ is greater but still small compared to τ_c. In this case u_{zf} equals zero initially due to the no-slip condition on the upper wall, grows at times compared to τ_f^f and then decays.

B. Velocity fluctuations

Figures 3 and 4 show $\langle u_z^2\rangle$ and $\langle u_\perp^2\rangle$ correspondingly as functions of vertical coordinate for various $m_{\max}$, t, N^0, and W. The initial maximum values of $\langle u_z^2\rangle$ is proportional to $N^{1/6}$ in accordance with Eq. (7) and fairly depends on the dimensionless container width. Initially the vertical fluctuations in

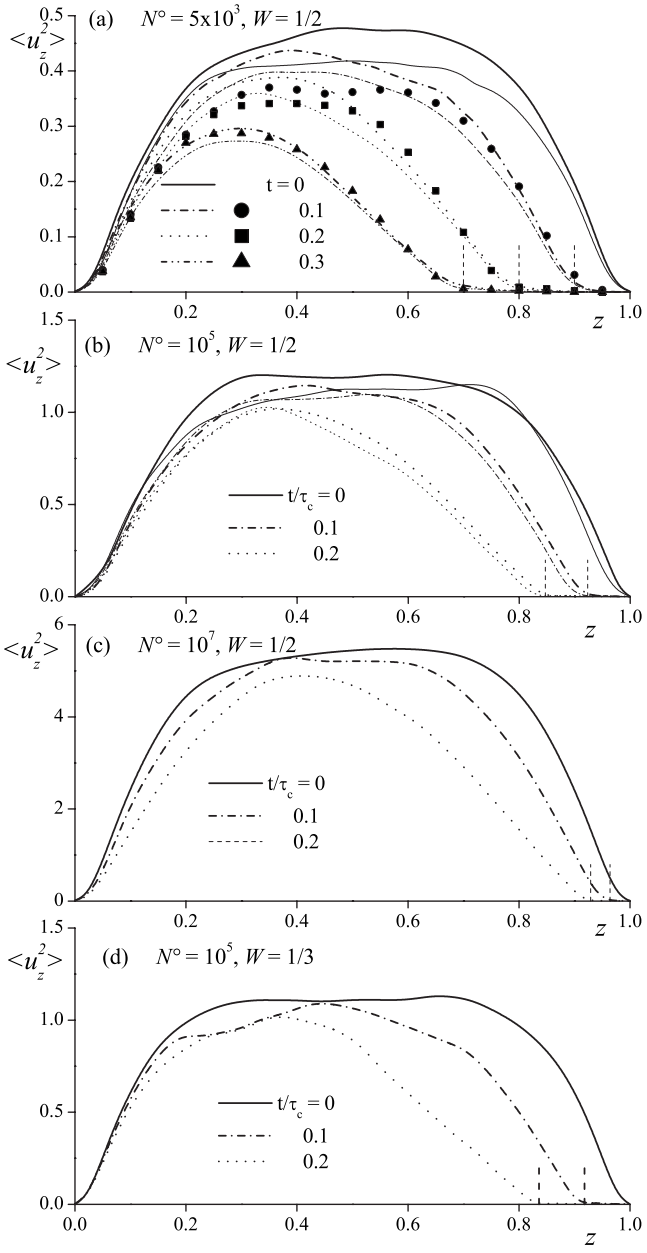

FIG. 3. Fluctuations of the vertical velocity $\langle u_z^2 \rangle$ in the full container as functions of z for various particle numbers and container widths. Dashed lines are the average sedimentation-front positions z_{f0} for (a) t=0.1, 0.2, 0.3, and (b)–(d) t/τ_c=0.1, 0.2. Bold lines correspond to the results obtained with $m_{\max}$=5, light lines in (a), (b) - with $m_{\max}$=4. (a) Symbols are the results obtained by the point-particle simulations [18] with $m_{\max}$=4.

the tall containers have plateaus in the middle parts, while the horizontal ones have maxima near the walls. The fluctuations are small in the clean fluid above the interface where the volume forces are zero. Both the vertical and horizontal fluctuations are small at the front. Therefore, the front acts, to the leading order, as a no-slip wall. u_{zf} is scaled like $N^{-1/2}$, so it is greater in the small container [see Fig. 3(a)]. The front deformations damp the velocity fluctuations in a layer near the interface of a thickness $O(W/2)$. In the bulk, the fluctuation decay is due to the convection of large particle clusters [2,9,14,15]. Heavier and lighter blobs convect to one of the two interfaces and are absorbed by the density gradient at the interface.

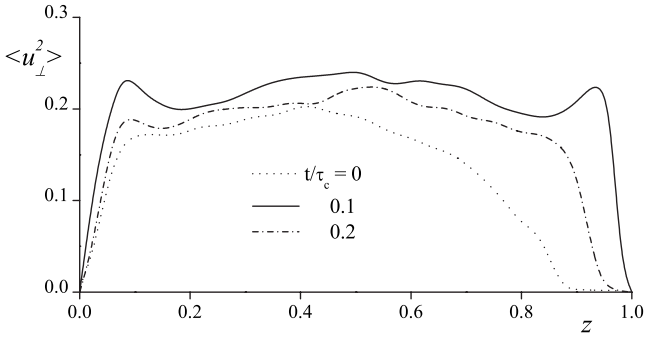

FIG. 4. Fluctuations of the horizontal velocity $\langle u_\perp^2 \rangle$ as functions of z.

The Fourier coefficients $\mathbf{u}^*$ are proportional to k^{-2} [see Eqs. (21) and (22)], so the dominant contributions to $\langle u_z^2 \rangle$ and $\langle u_\perp^2 \rangle$ come from small k, or from large-scale disturbances. The contributions of short-wave disturbances, which are due to microstructural rearrangements in the bulk, are small. It can be seen in Figs. 3(a) and 3(b) that the initial fluctuations calculated for $m_{\max}$=5 exceed only slightly those for $m_{\max}$=4, so the contributions of extra short-wave modes at t=0 are small indeed. The agreement of the dependences obtained with different $m_{\max}$ is even better for $t>0$. Therefore, the fluctuation decay is due to the convection of large-scale disturbances with length scales compared to the container width. The results for the small container [Fig. 3(a)] agree well with the point-particle simulations [18]. $\langle u_z^2 \rangle$ in the large containers decay faster because of the nonlinear convective effects. Significant decay is obtained in the largest container with $N^0=10^7$ [Fig. 3(c)] during a short time of the order of $0.1\tau_c$–$0.2\tau_c$, when the sedimentation front is still close to the upper wall. $\langle u_\perp^2 \rangle$ decay with time also but to a smaller degree than the vertical fluctuations. As a result the ratio $\langle u_z^2 \rangle / \langle u_\perp^2 \rangle$ diminishes with time in agreement with the experimental observations.

The convection decay mechanism can be illustrated for an artificial concentration field. Figure 5 shows the evolution of two large cubic blobs. The large concentration disturbances induce a strong counterclockwise vortex. The heavier and lighter blobs do not simply settle or rise but also interact with each other. The nonlinear convective terms in the continuity equation take into account blob changes due to the interactions. The significant transformations occur when the blobs are brought close together. When they approach the bottom wall and the front, their vertical velocities tend to the Stokes velocity, and the vortex stretches them in the horizontal direction. The stretching results in the extra decay of long-wave horizontal modes. Afterwards, the heavier blob deposits on the bottom wall. The lighter one is not absorbed but remains near the sedimentation front thus reducing the concentration in this region. For this reason lighter inhomogeneities are even more important for the decay. The accumulating of lighter and heavier blobs near the interfaces is also the cause of vertical stratification (see Sec. III D).

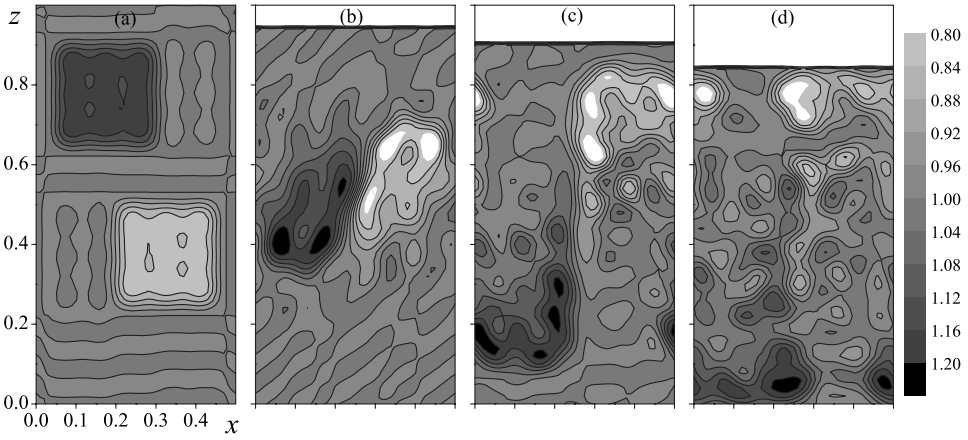

FIG. 5. Interaction of large heavy and light blobs. Concentration fields n/n_0^0 across the container width at (a)–(d) $t=0$, 0.05, 0.1, 0.15.

C. Comparison with experiments and linear continuum theory

The vertical velocity fluctuations are compared with the linear-theory predictions [20] and the experimental results [7]. The linearized solution similar to Eq. (11) was obtained for the case when both the concentration and fluid-velocity fluctuations are small:

$$\nu_1 = \nu_1^0(x,y,z+t), \quad \zeta = \varepsilon^{-1}\int_0^t u_{zf}d\tau, \quad \text{as } |\mathbf{u}| \ll 1. \quad (28)$$

The linear theory neglects the nonlinear terms, $\mathbf{u}\cdot\nabla\nu_1$ in Eq. (13) and $u_{xf}\frac{\partial\zeta}{\partial x}+u_{yf}\frac{\partial\zeta}{\partial y}$ in Eq. (14), i.e., it ignores the convective motion of lighter and heavier blobs. The initial disturbances ν_1^0 translate downward with the Stokes velocity $-\mathbf{e}_3$. However, the theory accounts for the front deformations ζ which are equal to the net number of particles passing through the basic-flow sedimentation front when $|\mathbf{u}| \ll 1$.

In the experiment [7], the mean vertical velocity $V_\parallel$ and the velocity variance relative to the mean $\sqrt{\langle u_z^2\rangle}/V_\parallel$ were measured for $a=3.7\times10^{-4}$, $\phi=0.0005$, $W=1/2$ which correspond to $N^0=5.89\times10^5$. The results were averaged over the viewing window, $0.275\leqslant z\leqslant 0.625$. Figure 6(a) compares the experimental and theoretical fluctuations $\langle u_z^2\rangle$ for the above N^0, ϕ, W averaged over the viewing window and over 100 runs. Initial values for the linear and nonlinear theories are the same within statistical error, as they correspond to the random Poisson particle distribution (27). In the experiment, the large values at short times can be attributed to a nonrandom initial density distribution. Both experimental dependences, $\sqrt{\langle u_z^2\rangle}/V_\parallel$ and $V_\parallel$, decay slowly at long times. As a result $\langle u_z^2\rangle$ evaluated from the data exhibit a faster decay, and no steady-state value is attained. The theories predict very weak decay initially when the sedimentation front is close to the upper container wall and far from the upper boundary of the viewing window. The point-particle simulations [9] also showed only small change in the fluctuations in a central sampling window at small times. The theoretical curve (solid line) agrees well with the experiment at $t>0.2$. The discrepancy between the present theory and the linear-theory predictions (dashed line) ignoring the convective effects is due to the blob convection. The effect is more pronounced for greater initial fluctuations. $\langle u_z^2\rangle$ is evaluated for the same container but greater concentration, $\phi=0.002$ [Fig. 6(b)]. The initial fluctuations are proportional to ϕ, so the nonlinear effects are greater in this case and result in faster decay. The difference between the two theories is significant at finite times and it grows with ϕ.

D. Average particle concentration

The vertical stratification of particle concentration has been studied recently [16,17,19] as a possible mechanism of fluctuation decay. The stratification in a dilute monosized suspension was attributed to the diffusion of the sedimentation front. The point-particle simulations [9,17] predict significant front broadening, while other simulations [15,18]

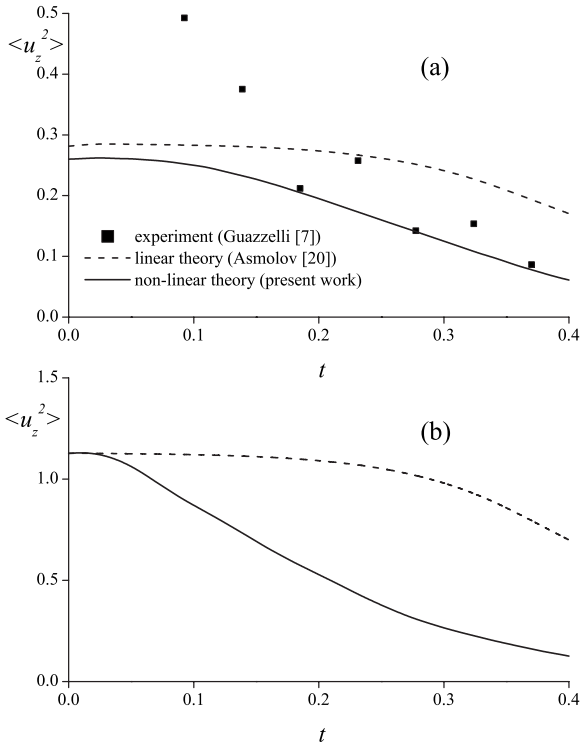

FIG. 6. (a) Comparison of the vertical-velocity fluctuations averaged over the viewing window with the experimental data by Guazzelli [7] for $\phi=0.0005$ and the linear-theory predictions [20]. (b) The difference between the two theoretical predictions is greater at $\phi=0.002$ because of the nonlinear convective effects.

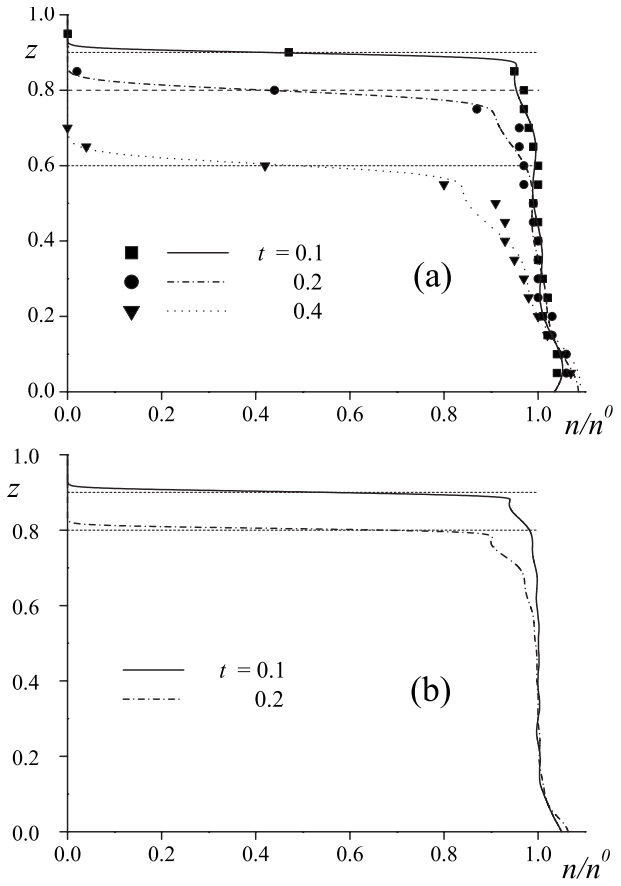

FIG. 7. Profiles $\langle n(z)\rangle$ for (a) cubic container, $W=1$, $N^0=5000$ and (b) thin container, $W=0.5$, $N^0=10^5$. Dashed lines are the average positions of the sedimentation front $z_{f0}(t)$. (a) Symbols are the predictions of the point-particle simulations [18].

gave a relatively small growth of the front width. In the middle part of container, only small vertical concentration gradient was obtained [14,15].

Within the continuum approach, a sharp interface between the suspension and the clean fluid is introduced. A side view of the deformations of the sharp front looks like the front diffusion, and this was the treatment of some space- or ensemble-averaged observations in the experiments and simulations.

The average concentration n is calculated using inverse Fourier transform and equation (9), i.e., $n(x,y,z)=0$ when the point is above the front, $z>z_f(x,y)$, and $n=n_0^0(1+\varepsilon\nu_1)$ for $z<z_f$. The results are averaged over 625 points, $x=0.04L_x i_x$, $y=0.04L_y i_y$, $1\le i_x, i_y \le 25$, in horizontal xy planes and over 100 runs. Figure 7(a) shows profiles $\langle n(z)\rangle$ calculated for various t in the medium cubic container, $W=1$, $N^0=5000$, using the continuum model. For comparison the results obtained by the point-particle simulations [18] are also shown. The agreement of the two approaches is good. The concentration gradient is large on the horizontally-averaged sedimentation front. The front width grows only slightly with time. Thus, there is no evidence of the diffusive spreading of the interface. Smaller gradient is obtained in the bulk. The stratification cannot be explained by the front diffusion as the concentration varies not only near the front but also near the bottom wall. It is due to the effects illustrated in Fig. 5. Heavy parts fall faster in the middle of the cell. As they approach the bottom wall, their velocities diminish and tend to the Stokes velocity because of the no-slip condition. They accumulate in this region, and the concentration increases there. Light blobs migrate toward the front. They remain in the vicinity of the front, in contrast to the heavier parts, which deposit on the bottom wall. As a result the deviation of the concentration from n_0^0 is greater near the front.

The profiles in the large tall container [Fig. 7(b)] are similar. The concentration gradient is small in the middle part of the container where the viewing windows in the experiments are located. The similar results were obtained by lattice-Boltzmann simulations [14,15] for dense suspensions. A relative width of horizontally averaged front scales like $(N^0)^{-1/2}$. So the horizontally averaged front is sharper in large containers, and the border between the front and the stratified region is more distinct. The front width does not vary with time.

IV. CONCLUSIONS

The evolution of the large-scale fluctuations of particle concentration and velocity in a sedimenting suspension has been simulated on the basis of the continuum model. The case when the fluctuations are comparable with the Stokes settling velocity has been studied. The equations governing the bulk concentration and sedimentation-front position have been derived using the perturbation methods with $\varepsilon \equiv N^{-1/2} \ll 1$. The approach has enabled us to avoid the problems due to the use of Fourier series for sharp concentration gradients and to sort the effects of the nonlinear coupling and the front deformations on the fluctuation attenuation.

The fluctuating sedimentation front is equivalent to surface forces acting on a fluid flow. The front holds position ensuring the dimensionless vertical fluid velocity across the front to be $O(\varepsilon)$. So it acts approximately as the no-slip wall. Its small, of order ε, deformations damp the velocity fluctuations in a layer of a thickness $O(W/2)$. The effect is greater for wide containers with a greater front area. The fluctuation decay in the bulk of tall containers is due to the convection. Large blobs migrate relative to the average concentration field and attain the suspension boundaries faster. They meet on their path other clusters more often and transform because of the nonlinear coupling. For this reason their attenuation is faster.

The horizontally averaged sedimentation fronts are sharp in large containers, and their width vary only slightly with time. There is no evidence of the diffusive spreading of the interface. The vertical stratification in the bulk is due to the nonlinear convective effects. Lighter and heavier particle clusters migrate across the container height and accumulate near the interfaces.

ACKNOWLEDGMENTS

The work was supported by the Russian Foundation for Basic Research (Grants No. 05-01-00847 and No. NSh-4272.2006.1).

[1] R. E. Caflisch and J. H. C. Luke, Phys. Fluids **28**, 759 (1985).
[2] E. J. Hinch, in *Disorder and Mixing*, edited by E. Guyon, J.-P. Nadal, and Y. Pomeau (Kluwer Academic, Dordrecht, 1988).
[3] H. Nicolai, B. Herzhaft, E. J. Hinch, L. Oger, and E. Guazzelli, Phys. Fluids **7**, 12 (1995).
[4] P. N. Segrè, E. Herbolzheimer, and P. M. Chaikin, Phys. Rev. Lett. **79**, 2574 (1997).
[5] S. Y. Tee, P. J. Mucha, L. Cipelletti, S. Manley, M. P. Brenner, P. N. Segrè, and D. A. Weitz, Phys. Rev. Lett. **89**, 054501 (2002).
[6] X. Lei, B. J. Ackerson, and P. Tong, Phys. Rev. Lett. **86**, 3300 (2001).
[7] E. Guazzelli, Phys. Fluids **13**, 1537 (2001).
[8] G. Bernard-Michel, A. Monavon, D. Lhuillier, D. Abdo, and H. Simon, Phys. Fluids **14**, 2339 (2002).
[9] L. Bergougnoux, S. Ghicini, E. Guazzelli, and E. J. Hinch, Phys. Fluids **15**, 1875 (2003).
[10] D. L. Koch and E. S. G. Shaqfeh, J. Fluid Mech. **224**, 275 (1991).
[11] A. J. C. Ladd, Phys. Fluids **9**, 491 (1997).
[12] F. Feuillebois, L. Talini, and J. Leblond, in *Continuum Models and Discrete Systems (CMDS9)*, Proceedings of the 9th International Symposium, Istanbul, Turkey, 1998, edited by E. Inan and K. Z. Markov (World Scientific, Singapore, 1998).
[13] A. J. C. Ladd, Phys. Fluids A **5**, 299 (1993).
[14] A. J. C. Ladd, Phys. Rev. Lett. **88**, 048301 (2002).
[15] N.-Q. Nguyen and A. J. C. Ladd, J. Fluid Mech. **525**, 73 (2005).
[16] J. Mucha and M. P. Brenner, Phys. Fluids **15**, 1305 (2003).
[17] P. J. Mucha, S.-Y. Tee, D. A. Weitz, B. I. Shraiman, and M. P. Brenner, J. Fluid Mech. **501**, 71 (2004).
[18] E. S. Asmolov, Fluid Dyn. (to be published).
[19] J. H. C. Luke, Phys. Fluids **12**, 1619 (2000).
[20] E. S. Asmolov, Phys. Fluids **16**, 3086 (2004).
[21] R. H. Davis and M. A. Hassen, J. Fluid Mech. **196**, 107 (1988).
[22] A. Levine, S. Ramaswamy, E. Frey, and R. Bruinsma, Phys. Rev. Lett. **81**, 5944 (1998).
[23] M. P. Brenner, Phys. Fluids **11**, 754 (1999).